ASEAN Journal for Science and Engineering in Materials

Journal homepage: https://ejournal.bumipublikasinusantara.id/index.php/ajsem

Advanced Design Considerations for Permanent Magnetic Bearings: Bibliometric Insights and the Effects of Axial Displacement and Shaft Sagging on Horizontal Overhung Systems

Azman Jamaludin[*]*, M Zarhamdy Md Zain, Nur Safwati Mohd Nor*

Universiti Teknologi Malaysia, Johor Bahru, Malaysia

[*]Correspondence: E-mail: azman56@graduate.utm.my

ABSTRACT

This study investigates the influence of axial displacement and shaft sagging on the performance of permanent magnetic bearings (PMBs) in horizontal overhung systems, supported by a bibliometric analysis of existing PMB research trends. The bibliometric review identifies dominant modelling approaches and reveals limited attention to axial displacement and shaft sagging effects in stacked PMB configurations. To address this gap, a modified analytical model based on Backers's magnetic scalar potential method is developed by incorporating axial displacement and shaft sagging into the design framework. The proposed model is validated through experimental investigation using a horizontal overhung rotor system. The results show that the combined effects of axial displacement and shaft sagging significantly alter magnetic alignment and reduce effective wavelength, leading to performance degradation. Statistical equivalence testing confirms strong agreement between the proposed formulation and established analytical models. The findings provide improved design guidance for enhancing PMB stability, reliability, and efficiency in practical rotating machinery applications.

ARTICLE INFO

Article History:
Submitted/Received 17 Oct 2025
First Revised 20 Nov 2025
Accepted 06 Jan 2026
First Available online 07 Jan 2026
Publication Date 01 Sep 2026

Keyword:
Air gaps (h_1),
Axial displacement,
Backers's works,
Shaft deflection,
Shaft flexibility factor.

1. INTRODUCTION

The design of permanent magnetic bearings (PMBs) is fundamentally governed by Earnshaw's principle, which states that a body cannot be stably levitated in all three spatial directions using static magnetic fields without active control or stabilizing mechanisms. This intrinsic limitation results in unavoidable degrees of freedom in both radial and axial directions, allowing rotor motion to occur during operation. Despite this constraint, PMBs have been widely adopted in rotating machinery due to their contactless operation, reduced mechanical wear, minimized lubrication requirements, and extended service life. Early developments of PMB technology were initiated by Baermann in 1954, with a comprehensive analytical foundation later provided by Backers using the magnetic scalar potential method, which remains a cornerstone in PMB design theory (Paden *et al*., 2003; Backers, 1960).

In horizontal overhung rotor systems, PMB performance is highly sensitive to geometric imperfections arising from axial displacement, shaft sagging, shaft deflection, and bearing misalignment. These effects generate angular misalignment between stacked magnetic rings, distort air-gap distributions, and reduce effective magnetic wavelength, which in turn degrades magnetic pressure and bearing efficiency. While many PMB models assume ideal alignment between inner and outer magnetic rings, practical operating conditions frequently introduce deviations due to external disturbances such as load variations, thermal effects, shaft bending, and differential bearing wear. The contrast between ideal ring alignment and misaligned configurations in real PMB systems is illustrated in **Figure 1**, highlighting the discrepancy between theoretical assumptions and actual operating conditions.

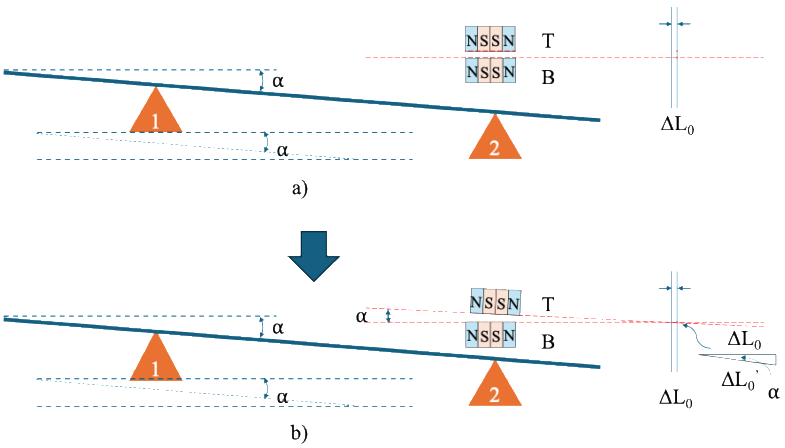

Figure 1. Configuration of stacked rings for PMB (a) Both rings in pure parallel (b) Both rings are not in parallel.

The presence of axial displacement combined with shaft sagging further amplifies ring misalignment, resulting in a significant reduction in effective magnetic wavelength, as illustrated in **Figure 2**. This phenomenon directly reduces magnetic force and pressure, thereby lowering PMB efficiency and operational stability. Despite the growing body of PMB research focusing on improving stiffness through stacked ring configurations, limited attention has been given to the combined effects of axial displacement and shaft sagging on PMB performance in horizontal overhung systems.

Therefore, this study aims to address this critical limitation by developing an enhanced analytical model that incorporates axial displacement and shaft sagging into PMB design considerations for horizontal overhung systems. Supported by experimental validation and bibliometric insights, this work seeks to establish practical design limits and performance

criteria to improve PMB stability, reliability, and efficiency under realistic operating conditions.

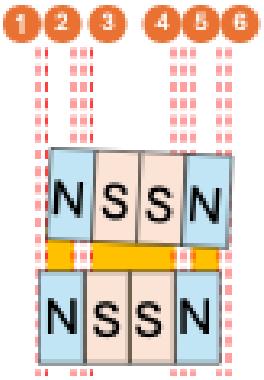

Figure 2. Six-time axial displacements with shaft sagging.

2. LITERATURE REVIEW

2.1. Fundamental Theories and Analytical Models of PMBs

The theoretical foundation of PMB design originates from Earnshaw's theorem, which defines the inherent instability of static magnetic levitation systems. Building on this principle, Backers developed one of the earliest and most influential analytical models for PMBs using the magnetic scalar potential approach, enabling the calculation of magnetic force, pressure, and stiffness between concentric magnetic rings (Backers, 1960). This model assumes ideal geometric alignment and uniform air gaps, as illustrated in **Figure 3**, and has been widely adopted as a baseline for subsequent PMB research.

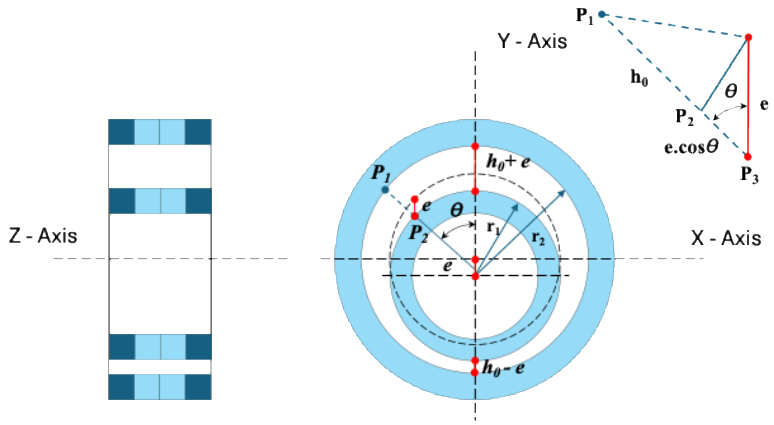

Figure 3. Backers model for a PMB without axial displacement and shaft sagging.

Backers clarified the eccentricity of the rings, determined by the distance from P1 to P3, which includes the relationships between the initial air gaps and the eccentricities of both the outer and inner rings, as specified in Equation (1). The integration of magnetic pressure in the rings measures the magnetic force applied to the PMB. A revision of the current mathematical model will be undertaken to address existing deficiencies in the proposed extension of the Backers' model.

$$h_1 = h_0 + e.cos\,\theta \quad (1)$$

Subsequent studies expanded on Backers's work by introducing alternative analytical approaches. Yonnet applied the virtual work principle to evaluate magnetic force, stiffness, and torque for PMBs under axial and radial magnetization, providing improved flexibility in

PMB modeling (Yonnet, 1981). Other study utilized the Coulomb method to optimize structural parameters for axially stacked PMBs, demonstrating enhanced stiffness characteristics through optimized ring arrangements (Moser *et al*., 2006). Further extended the Coulomb-based approach by developing empirical analytical models that account for both axial and radial magnetization effects on PMB load capacity (Ravaud *et al*., 2009a; Ravaud *et al*., 2009b).

2.2. Numerical, MATLAB-Based, and FEM Approaches

Although analytical models provide valuable insights into PMB behavior, they often involve complex integrals and computational challenges. Wang et al. highlighted the limitations of purely analytical approaches due to the absence of corresponding numerical solutions in early PMB studies (Wang *et al*., 2003). With advancements in computational tools, MATLAB-based symbolic and numerical integration techniques became widely used to derive analytical solutions more efficiently, particularly for magnetic scalar potential models (Paden *et al*., 2003).

In recent years, finite element method (FEM) simulations have gained prominence due to their ability to capture complex magnetic field distributions and structural interactions with higher accuracy. Other studies demonstrated the effectiveness of FEM-based approaches in analyzing PMB stiffness, load capacity, and dynamic behavior under various operating conditions (Zhang *et al*., 2011; Lijesh *et al*., 2016). However, Zhang *et al*. (2019) emphasized that FEM simulations require well-defined initial geometrical parameters, underscoring the continued importance of analytical models in early-stage PMB design.

2.3. Experimental Studies and Structural Misalignment Effects

Experimental investigations have played a critical role in validating PMB analytical and numerical models. Tian et al. developed an analytical model using virtual work and superposition principles and validated it through experimental studies, highlighting the sensitivity of PMB performance to magnetization direction and air-gap variation (Tian *et al*., 2012). Other studies reported that external disturbances such as shaft deflection, bearing wear, and thermal expansion can significantly alter PMB air gaps and alignment, leading to reduced performance and increased vibration (Wang *et al*., 2023).

However, most experimental studies assume either negligible axial displacement or isolated effects of shaft deflection, without explicitly addressing their combined influence. The misalignment induced by axial displacement and shaft sagging in stacked PMB configurations, as shown in **Figure 1(b)**, remains insufficiently explored in existing literature.

3. METHODS

This study adopts an analytical–experimental approach to investigate the effects of axial displacement and shaft sagging on the performance of PMBs in a horizontal overhung system. The methodology consists of three main stages: (i) formulation of an enhanced analytical model based on Backer's magnetic scalar potential theory, (ii) numerical implementation and parametric evaluation using MATLAB, and (iii) experimental validation through a constructed test rig designed to replicate realistic operating conditions. The following **Table 1** is to ensure the written scientific terms, concepts, and consensus for enabling effective communication and understanding within this paper.

Table 1. Nomenclature.

Symbol	Definition
L_{2A}	Bearing Span - 491.355 mm
L_{2B}	Bearing Span - 390.855 mm
L_{2C}	Bearing Span - 290.855 mm
$Ø$	Diameter
ΔL_o	Initial axial displacement
ΔL_A	Axial displacement A
ΔL_B	Axial displacement B
ΔL_C	Axial displacement C
h_0	Initial air gaps
h_1	Final air gaps
e	Shaft eccentricity
e'	Extension of shaft eccentricity
σ	Stress
M_1	Magnetization ring 1
M_2	Magnetization ring 2
μ_0	Vacuum permeability
d	Ring thickness
λ	Wavelength
r	Means ring radius
r_1	Inner ring radius
r_2	Outer ring radius
F_m	Magnetic force
P_m	Magnetic pressure
L_1	Bearing span length
L_2	Overhung length
D_1	Diameter bearing
D_2	Diameter overhung
°	Degree
α	Angle of shaft sagging.
df	Statistically degree of freedom
p-value	The probability statistical measure
mm	millimeter
K	Stiffness
kN	kilo Newton
kOe	kilo Orsted equivalent
MGOe	Mega Gauss Orsted equivalent
MPa	Mega Pascal
SFF	Shaft Flexibility Factor

3.1. Analytical Formulation of the PMB Model

Backers established that the fundamental Equation (2) in his research derives from magnetic potential energy and the configuration of a magnetic dipole, which derived the integration of magnetization for the inner ring M_1 and the outer ring M_2 in a vacuum, considering the permeability μ_o and the ratio of the thickness d of the rings to the air gap with wavelength λ. The two rings are separated by air gaps (h_o).

$$\sigma = \left(\frac{M_1 M_2}{2\mu_0}\right)\left(1 - \frac{1}{e^{\left(\frac{2\pi d}{\lambda}\right)}}\right)^2\left(\frac{1}{e^{\left(\frac{2\pi h_0}{\lambda}\right)}}\right) \quad (2)$$

where both rings are magnetized at the same amplitude for M_1 and M_2 with spatial frequency for m and n, but at different periodic magnetization and phase as described in Equations (3) and (4). The phase is shifted by a displacement at z0, which is commonly shifted at $\lambda/2$.

$$M_1(z) = \frac{4M_0}{\pi} \sum_{m=1,3,5,7....}^{\infty} \frac{\cos\left(\frac{m2\pi(z)}{\lambda}\right)}{n} \quad (3)$$

And for the inner ring for M2 at equation (4)

$$M_2(z) = \frac{4M_0}{\pi} \sum_{n=1,3,5,7....}^{\infty} \frac{\cos\left(\frac{n2\pi(z+z_0)}{\lambda}\right)}{n} \quad (4)$$

In reality, various uncertainties prevail: the true geometry of the PMB set is always of a ring misaligned due to the presence of axial displacement, shaft bending, deflection, material properties affected by thermal conditions, alignment inaccuracies, or differential wear on the supporting bearings leading to shaft sagging. The consequences of shaft sagging and axial displacement will increase the ring misalignment between the inner and outer rings that form in stacked magnetic rings. It will reduce the magnetic pressure that precipitated the failure of the PMB. **Figure 4** demonstrates that the initial axial displacement ΔL_o leads to the actual axial displacement ΔL, which is affected by the angle α and the eccentricity e' between P1 and P1'.

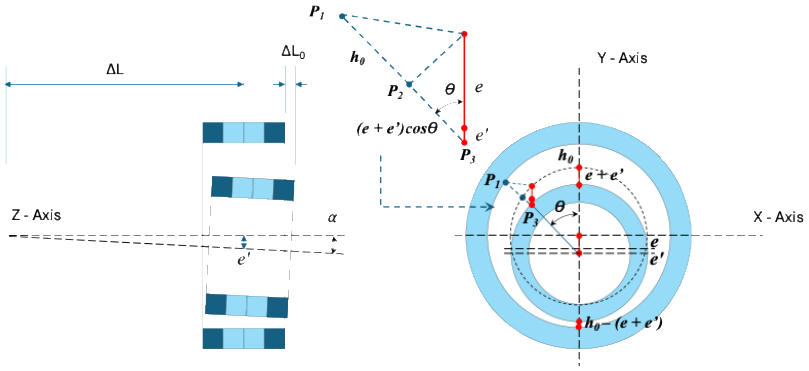

Figure 4. PMB model with the existence of axial displacement and shaft sagging.

Through the positioning approach, the air gap h_1 is defined in Equation (5), consisting of shaft eccentricity e, extension of shaft eccentricity e', and initial air gap h_0. e' is propagated to the increment of shaft sagging and the length of initial axial displacement.

$$h_1 = h_0 + (e + e').cos\theta \quad (5)$$

Substituting Equation (5) into Equation (2), the following Equation (6) for air gap h1, axial displacement, and shaft sagging can be found

$$\sigma = \left(\frac{M_1 M_2}{2\mu_0}\right)\left(1 - \frac{1}{e^{\left(\frac{2\pi d}{\lambda}\right)}}\right)^2 \left(\frac{e^{\left(\frac{2\pi(e+e')cos\theta}{\lambda}\right)}}{e^{\left(\frac{2\pi h_1}{\lambda}\right)}}\right) \quad (6)$$

Integrating Equation (6) over the radius of r = (r_2 - r_1) / 2 and angle θ for the range of -π/2 to π/2 to define the volume of repulsive force (F) acted on the PMB rotor as illustrated in Equation (7):

$$\frac{F}{2\lambda r} = \left(\frac{M_1 M_2}{2\mu_0}\right)\left(1 - \frac{1}{e^{\left(\frac{2\pi d}{\lambda}\right)}}\right)^2 . \frac{1}{e^{\left(-\frac{2\pi h_1}{\lambda}\right)}} . \left(\frac{\lambda r}{2\pi}\right) \int e^{\left(\frac{2\pi(e+e')cos\theta}{\lambda}\right)} . cos\theta d\theta \quad (7)$$

By taking magnetic pressure P_m = F/2λr, and since M_1 and M_2 are arbitrary periodic functions of an infinite sum of m∈ {1,2,3,…∞} and n∈ {1,2,3,….∞}, it has a Fourier series representation. Decomposing the function into a weighted sum for the interval $[\frac{-\lambda}{2}, \frac{\lambda}{2}]$, the magnetic pressure acting between outer and inner rings is found as Equation (8):

$$P_m = \frac{4B_r^2}{\mu_0}\sum_{n=1,3,5,7\ldots}^{\infty}\left(\frac{\left(\frac{1}{e^{\left(-\frac{n2\pi h_1}{\lambda}\right)}}\right)\left(1-\frac{1}{e^{\left(\frac{n2\pi d}{\lambda}\right)}}\right)^2 I\left(\frac{n2\pi(e+e')}{\lambda}\right)}{n^2}\right) \quad (8)$$

3.2. Design of Radial Magnetic Bearing for Overhung System

The application of Equation (8) in MATLAB has been carried out for samples N35, N38, N40, N42, N48, N50, N52, and N54, under the condition of zero axial displacement. It has been observed that all maximum magnetic pressures (Pmax) occur when (h1/λ) is equal to 0.22. This value exceeds π/2, as indicated in Baker's work, which is based on numerical calculations as described in **Figure 5**.

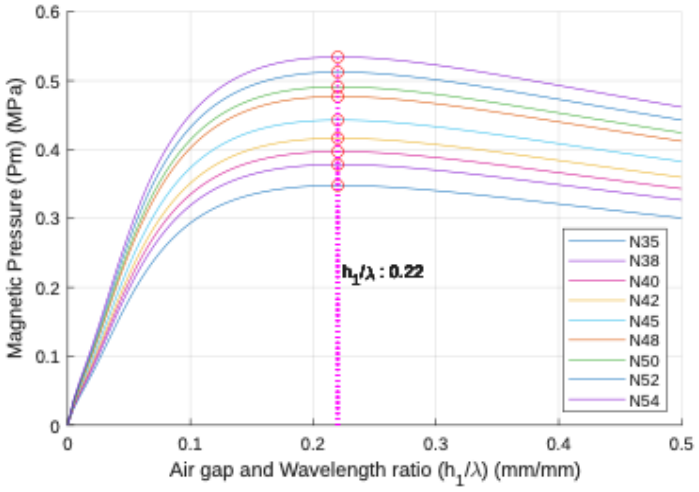

Figure 5. Magnetic Pressure vs Airgap-wavelength ratio for N35,38,40,42,45,48,50,52 and 54.

The model is compared with the previous research (Tian *et al*., 2012), which employed virtual work with superposition for PMB. MATLAB is utilized to simulate the processes related to various grades of neodymium as described in **Table 2**. The hypothesis test utilizes an unpaired t-test of the alternative hypothesis, with a p-value of 0.9816 indicates the rejection of the null hypothesis based on conventional criteria. The Two-Sample Equivalence Test (TOST) has been considered for a confidence interval of α at least 0.1 underpins the margin of error in the magnetic pressure for these two models, with a 90% confidence interval (-0.05225, 0.050871) that is wholly contained within the interval range (-0.1, 0.1) and defines that the two outcomes are considered equivalent.

3.3. External Disturbance

Three primary external disturbances may influence the results of PMB air gap measurements: shaft deflections, shaft flexibility factor (SFF), and material selection.

3.3.1. Shaft deflection

In addition to axial displacement and shaft sagging, shaft deflection has been quantified as a factor influencing rotor behaviour. Macaulay's method is employed to estimate the bending moment (m), the material property of Young's modulus (e), and the moment of inertia (I) of the shaft's cross-section, as delineated in the Euler-Bernoulli beam theory. Twenty-four

points are employed in **Figure 6** to evaluate the shaft characteristics under different loads at point 23. PMB is measured at three different bearing spans, and two reaction forces, R1 and R2, can be discerned based on varying bearing spans for "No-load" and "Load" at point 23. The estimations of R1 and R2, obtained from shaft deflections, will be utilized to assess external disturbances that may affect the air gap results for PMB.

Table 2. Comparison of virtual work and magnetic scalar model for magnetic pressure.

Magnet Grade	Magnetic Pressure (MPa) Virtual Work Model	Magnetic Pressure (MPa) Magnetic Scalar Model
N35	0.3481	0.3470
N38	0.3792	0.3773
N40	0.3979	0.3961
N42	0.4162	0.4153
N45	0.4423	0.4417
N48	0.4772	0.4758
N50	0.4923	0.4897
N52	0.5152	0.5111
N54	0.5353	0.5329

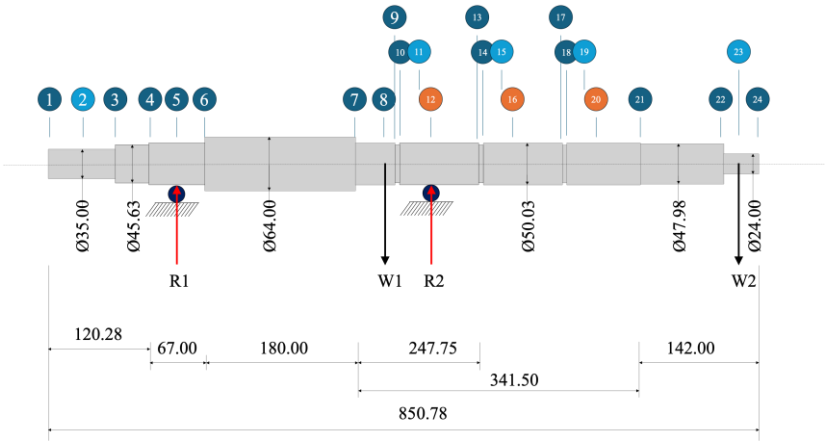

Figure 6. The overall geometry of the shaft with points for assessing shaft deflections. All measurements unit in mm.

It was noted under "No-load" that the PMB for ΔL2A is 491.355 mm, and the shaft deflection at point A is 0.246 mm. PMB for ΔL2B is 390.855 mm, with a shaft deflection at point B of 0.172 mm; PMB for ΔL2C is 290.855 mm, with a shaft deflection at point C of 0.149 mm, as depicted in **Figure 7**.

Under the "Load" condition, the PMB for ΔL2A measures 491.355 mm, and the shaft deflection at point A is 0.179 mm. The PMB for ΔL2B is 390.855 mm, demonstrating a shaft deflection of 0.132 mm at point B, whereas the PMB for ΔL2C is 290.855 mm, with a shaft deflection of 0.114 mm at point C, as depicted in **Figure 8**.

3.3.2. Shaft flexibility factor (SFF)

Another significant factor affecting external disturbances is the air gap for PMB: shaft bending in the overhung section, determined by the beam deflection Equation (9). Deflection (Y) is proportional to the length of overhang at $L1^3$ and inversely proportional to the area moment of inertia (I) for the diameter of shaft D4. Since load (W), material property for Young's modulus (E), and coefficient (C) are constant, $L1^3$ and $D1^4$ ratios serve as the benchmark for the shaft flexibility factor for an overhung system.

$$Y = \left(\frac{W}{C.E.\left(\frac{\pi}{64}\right)}\right).\left(\frac{L_1^3}{D_1^4}\right) \quad (9)$$

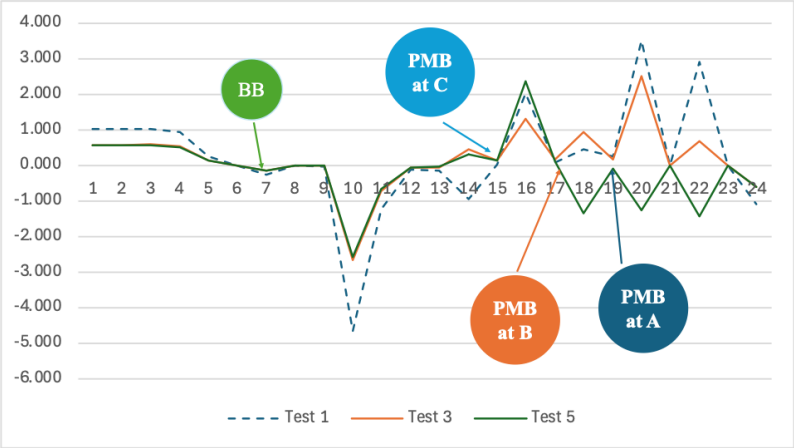

Figure 7. Deflection for No-load for tests 1,3,5 for PMB at Points 15,17, and 19.

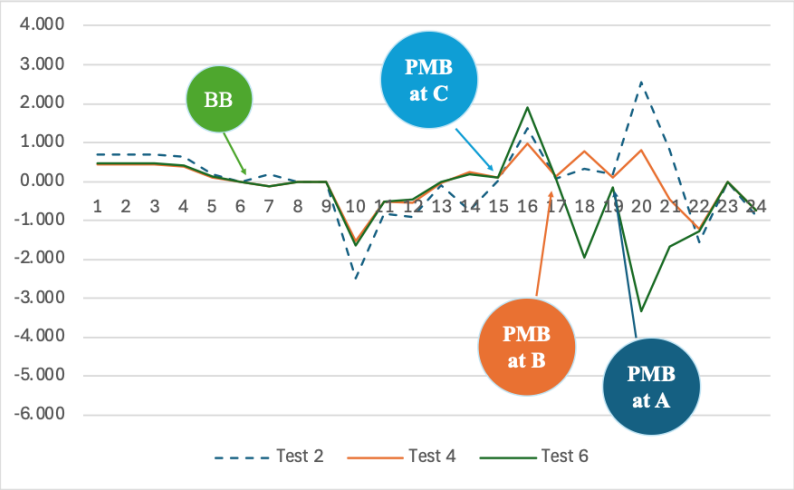

Figure 8. Deflection for Load for test 2,4,6 for PMB at Points 15,17, and 19.

The extension of overhung deflection for the SFF can be described by the model as described in **Figure 9**.

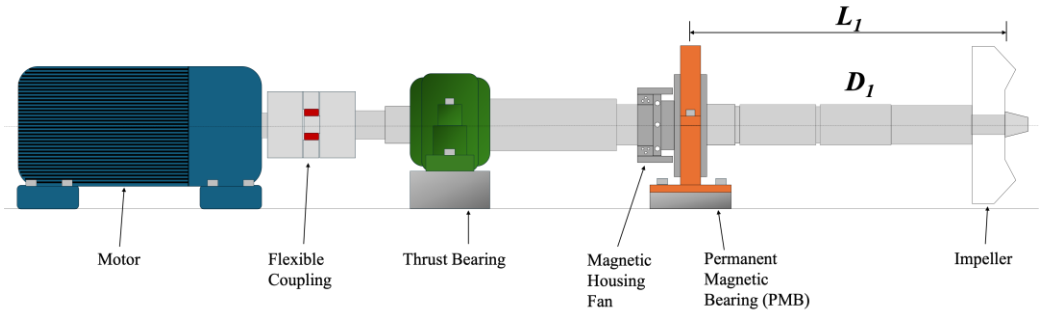

Figure 9. Schematic drawing for an overhung shaft assembly for L_1 and D_1.

The overall SFF is formulated according to Equation (10), which represents the stiffness of the rotor system, which adds complexity to the forces that influence the system.

$$SFF = \frac{L_1^3}{D_1^4} \quad (10)$$

It is crucial to identify stiffness for a specific shaft diameter at points A, B, and C. For a diameter of Ø50.049 mm, stiffness at A, B, and C will be at 99106.29, 65185.29, and 48625.04 MPa, respectively. Furthermore, similar stiffness across the point can be obtained by increasing the shaft diameter, like C can be improved to the stiffness similar to B by increasing the diameter to Ø54.30 mm, as illustrated in **Figure 10**.

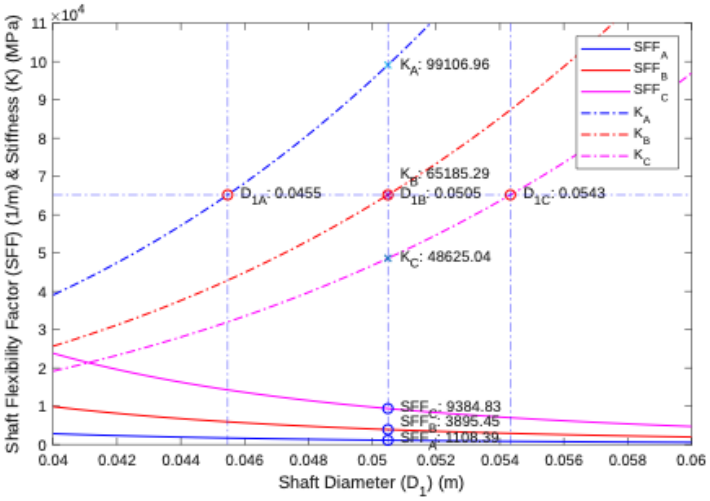

Figure 10. Shaft flexibility factor and Stiffness (K) for points A, B, and C.

3.4. Material

A grade N35 Neodymium magnet axially magnetized has been chosen for a PMB with (mm) with Residual Magnetism (Br) at 117000 gauss (G), Cohesive Strength 10.8 kOe, Energy Product 33 MGOe, and Maximum operating temperature below 80 degrees Celsius (°C). The PMB housing is designed for interchangeability, installation simplicity, and elevated stiffness at the rotor. A Stainless steel 304 cartridge design consists of a rotating shaft sleeve and setting plates. A design to efficiently separate the rotating and stator rings. The rotating sleeve is designed to compensate for misalignment, and the shaft is fabricated from round rolled non-metallic steel (forgings) with a diameter of Ø64 mm to withstand bending moments and torque. Marine grade according to DIN 1.4401, X5CrNiMo17-12-2, 316S16, Z6CND17.11, SUS316, 2347, assessed based on load capacity, wear resistance, corrosion resistance, temperature stability, thermal expansion, machinability, and maintainability. Thrust bearing housing FAG SAV 890 Split Plummer block housing, Cast-iron material, two-piece housing configuration through shaft mounting arrangement with NTN7210B angular contact ball bearings arrangement. Some reports (Yonnet,1981) cite that the axial load from the system is found at 1.140 kN. Plotting the axial load to NTN7210B angular contact ball bearings is found that axial displacement is 0.0075 mm. 2.5 kN will produce axial displacement at 0.016 mm, and the thrust bearing is capable of operating up to 11 kN for bearing bore Ø50.00. An Aluminum flexible coupling 44 X 40 mm is attached to the rotor. A skid of 142 kilograms (kg) of base of mild steel, size of 1505 X 480 mm.

3.5. Instrument

Temperature was measured by a Casio thermometer DQD-80J with accuracy ± 1°C. The set of instruments has been used for measuring Air Gap (h1) and alignments with Insize Digital Caliper 1108-200 range of 0-200mm with accuracy ± 0.03 mm and Mitutoyo 500-501-10 accuracy ± 0.05 mm. Shaft Parallelism and bearing alignment have been used Shane digital

dial indicator 5307 range 0 – 12.7 mm, with accuracy ± 0.03 mm, and a Mitutoyo dial gauge 513-401-10E with resolution 0.001 mm, with accuracy ± 0.003 mm.

3.6. Model Contruction and Test Plan

A rig is constructed to evaluate the shaft sagging and axial displacement in a two-bearing system within PMB. The rig utilizes two angular contact ball bearings configured in a back-to-back arrangement at point 5. PMB is designed for non-locating bearings. Three distinct bearing spans for L2A, L2B, and L2C; axial displacements ΔLA, ΔLB, and ΔLC; and shaft sagging angles αA, αB, and αC as depicted in **Figure 11**.

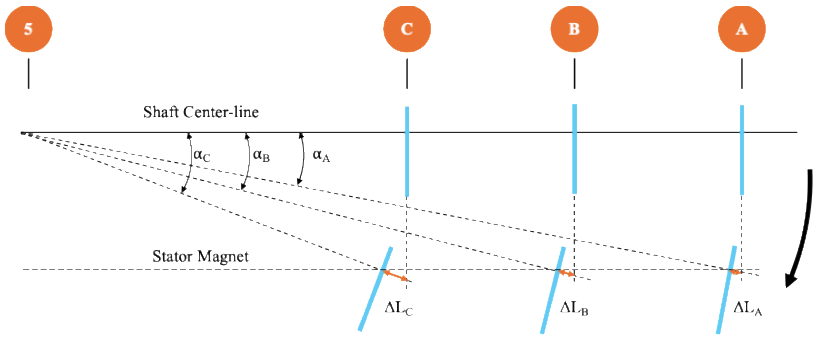

Figure 11. The plan for addressing different axial displacements and shaft sagging.

A rotor with a diameter of 50 mm and a mass of 18 kg with a three-phase 0.75kw motor and a Variable Frequency Drives (VFDs) that control the speed and torque of the motor by adjusting the frequency and voltage of the power supplied as described in **Figure 12**.

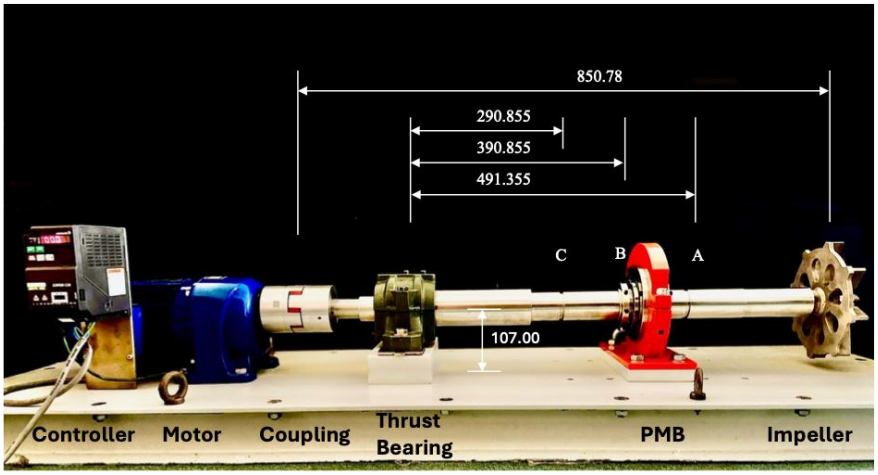

Figure 12. Overhung system with radial magnetic bearing for side view. All measurements unit in mm.

Thirty-six tests are scheduled, utilizing three distinct bearing spans, ΔL_{2A} = 491.355 mm, ΔL_{2B} = 390.855 mm, and ΔL_{2C} = 290.855 mm, and “Load” and “No-load”. There will be six varying reactions at PMB: 71.767, 74.800, 87.927, 91.846, 115.092, and 120.351 N Deflections at PMB, SFF at 9348, 3895, and 1180 1/m, and Un Couple and Couple with Motor as depicted in **Table 3**. The test is labeled as 1As, 2As, 3Bs, 4Bs, 5Cs, and 6Cs for static simulation for RPM 0, 1Aa, 2Aa, 3Ba, 4Ba, 5Ca, and 6Ca for Un Couple and the rest test is labels from 1 to 18 is the test with various contrition with different reaction forces, deflections, SFF, Speed in couple with drive.

Table 3. The compilation of external disturbances for PMB encompasses data on reaction forces, shaft deflection at PMB, Maximum Shaft Deflection, SFF, Speed, and Reaction Force.

Test No	Reaction Force (N)	Speed (rpm)	SFF $1X10^3$ (1/m)	Type
1As	0.00	0	0.000	Un Couple
1Aa	71.77	0	9.384	Un Couple
1Ab	71.77	0	9.384	Couple
1	71.77	90	9.384	Couple
2	71.77	160	9.384	Couple
3	71.77	250	9.384	Couple
2As	0.00	0	0.000	Un Couple
2Aa	74.88	0	9.384	Un Couple
2Ab	74.88	0	9.384	Couple
4	74.88	90	9.384	Couple
5	74.88	160	9.384	Couple
6	74.88	250	9.384	Couple
3Bs	0.00	0	0.000	Un Couple
3Ba	87.93	0	3.895	Un Couple
3Bb	87.93	0	3.895	Couple
7	87.93	90	3.895	Couple
8	87.93	160	3.895	Couple
9	87.93	250	3.895	Couple
4Bs	0.00	0	0.000	Un Couple
4Ba	91.85	0	3.895	Un Couple
4Bb	91.85	0	3.895	Couple
10	91.85	90	3.895	Couple
11	91.85	160	3.895	Couple
12	91.85	250	3.895	Couple
5Cs	0.00	0	0.00	Un Couple
5Ca	115.09	0	1.108	Un Couple
5Cb	115.09	0	1.108	Couple
13	115.09	90	1.108	Couple
14	115.09	160	1.108	Couple
15	115.09	250	1.108	Couple
6Cs	0.00	0	0.00	Un Couple
6Ca	120.35	0	1.108	Un Couple
6Cb	120.35	0	1.108	Couple
16	120.35	90	1.108	Couple
17	120.35	160	1.108	Couple
18	120.35	250	1.108	Couple

4. RESULTS AND DISCUSSION

PMB capacity characteristics strongly depend on its structural dimensions, especially the air gap between the magnetic rings. A thickness-to-wavelength ratio (d/λ) of 1.0 is established, with the thickness (d) set at 10 mm. The study also considers the axial and radial dimensions of the magnetic rings, as well as the spatial positioning of the inner and outer rings.

4.1. Analytical Simulation of PMB Capacity Characteristics Result

The PMB capacity is quantitatively defined by an initial axial displacement of 0.008 mm, derived from laboratory measurements, which closely aligns with the 0.0075 to 0.013 mm displacement recorded for NTN7210B angular contact ball bearings. The impact of structural parameters on PMB capacity is examined for ΔL2A = 491.355 mm, ΔL2B = 390.855 mm, and ΔL2C = 290.855 mm for "Load" and "No Load" based on deflection displacement at the PMB sleeve. The magnetic pressures are reduced proportionally to the increment of shaft sagging, while increasing the load will increase the shaft sagging as described in **Figure 13**.

4.2. Analytical Simulation of PMB Capacity Characteristics Result

To verify the accuracy of the Analytical Simulation of PMB Capacity Characteristic, the PMB is experimentally studied in both radial and axial displacement and shaft sagging. Air gaps and shaft sagging are measured for each location at A, B, and C, the positioning method with load and unload, couple and uncouple, and at different speeds at 90.160 and 250 RPM. The findings are presented in **Table 4**.

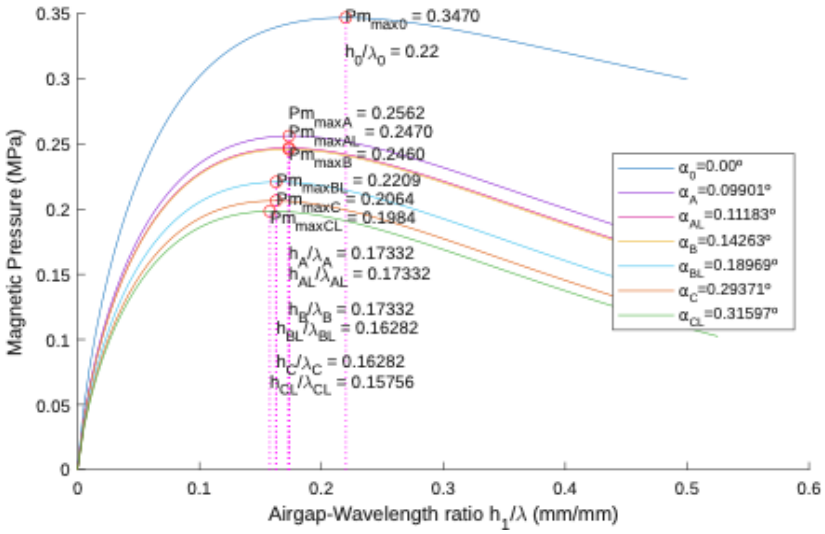

Figure 13. Magnetic Pressure (Pm) for air gaps-wavelength ratio (h1/λ).

Table 4. Axial displacement, Air Gaps, Shaft sagging for Analytical simulation and experimental results.

Test No	Speed (RPM)	ΔL_0 $1x10^{-2}$ (mm)	Sag $1x10^{-2}$ (°)	Air Gaps (mm)	Peak Vibration (mm/s)
1As	0	8.0591	8.8855	1.395	0.000
1Aa	0	8.0591	8.8855	1.238	0.000
1Ab	0	8.0591	8.8855	1.238	0.000
1	90	8.0596	8.9205	1.235	1.110
2	160	8.0599	8.9438	1.233	1.566
3	250	8.0599	8.9438	1.233	2.240
2As	0	8.0603	8.9788	1.395	0.000
2Aa	0	8.0603	8.9788	1.230	0.000
2Ab	0	8.0599	8.9438	1.233	0.000
4	90	8.0600	8.9555	1.232	0.460
5	160	8.0600	8.9555	1.232	0.671

Table 4 (continue). Axial displacement, Air Gaps, Shaft sagging for Analytical simulation and experimental results.

Test No	Speed (RPM)	ΔL_0 $1x10^{-2}$ (mm)	Sag $1x10^{-2}$ (°)	Air Gaps (mm)	Peak Vibration (mm/s)
6	250	8.0602	8.9671	1.231	0.938
3Bs	0	8.0786	11.4927	1.395	0.000
3Ba	0	8.0786	11.4927	1.216	0.000
3Bb	0	8.0757	11.2728	1.231	0.000
7	90	8.0759	11.2875	1.230	0.386
8	160	8.0757	11.2728	1.231	0.542
9	250	8.0757	11.2728	1.231	0.780
4Bs	0	8.0790	11.5220	1.395	0.000
4Ba	0	8.0811	11.6686	1.204	0.000
4Bb	0	8.0757	11.2728	1.231	0.000
10	90	8.0759	11.2875	1.230	0.333
11	160	8.0777	11.3475	1.231	0.475
12	250	8.0777	11.3475	1.225	0.672
5Cs	0	8.1216	16.5669	1.395	0.000
5Ca	0	8.1216	16.5669	1.159	0.000
5Cb	0	8.1242	16.7442	1.150	0.000
13	90	8.1242	16.7442	1.150	1.276
14	160	8.1317	17.2366	1.125	1.817
15	250	8.1347	17.4336	1.115	2.596
6Cs	0	8.1213	16.5472	1.395	0.000
6Ca	0	8.1213	16.5472	1.160	0.000
6Cb	0	8.1347	17.4336	1.115	0.000
16	90	8.1353	17.4730	1.113	1.482
17	160	8.1387	17.6897	1.102	2.149
18	250	8.2006	21.2749	0.920	-

4.3. Comparison of Analytical Simulation and Experimental Results

A comparative analysis of air gap and shaft sagging characteristics was conducted to validate the accuracy of the modelling and design structural parameters through both analytical simulations, Experimental (uncoupled), and Experimental (coupled with Speeds). The investigation results in **Figure 14** illustrate the overall data with labels 1. Analytical Simulation, 2. Experimental (Uncouple) and 3. Experimental (Couple and Speed). It can be concluded that the errors in shaft sagging escalate with increasing axial displacement, and this data offset varies linearly, signifying a persistent linear discrepancy between the analytical simulation and experimental data. The details of each test will be evaluated to define the error.

4.3.1. Evaluation of test A for analytical simulation, experimental (no couple), and experimental (couple and speed)

Experimental Test A for Experimental (Couple) indicates that the shaft sagging data falls between the values observed in Experimental (Un Couple), specifically ranging from 0.0888 to 0.08898°. This test highlights the consistency of alignment, showing proximity during both rotor load and no-load conditions, and it reflects the changes in speed as illustrated in **Figure 15**.

From SFF's viewpoint, the system exhibits greater stiffness than B and C, with a stiffness constant K measured at 99,106.96 MPa. This measurement indicates the consistency of the data between Experimental (Couple) and Experimental (Un Couple). The Experimental (Couple) is evaluated against the analytical simulation utilizing an unpaired t-test. The two-tailed p-value is below 0.0001, and the 95% confidence interval spans from 0.160157 to 0.163493. The computed t-value is 208.0655, accompanied by 14 degrees of freedom (df) and a standard error of difference of 0.001 mm. The low p-value signifies that, according to conventional standards, this difference is deemed highly statistically significant and dependable. The rise in peak vibration for the system during no-load operation correlates with a deflection of 4.5 mm at point 10 of the rotor system. Comprehensive evaluations demonstrate that the data is reliable and consistent with the analytical simulation. Point A demonstrates optimal alignment and possesses a superior stiffness structure for PMB; however, the significant deflection of the rotor adversely affects its overall stability, and it is not stable for an overhung rotor system.

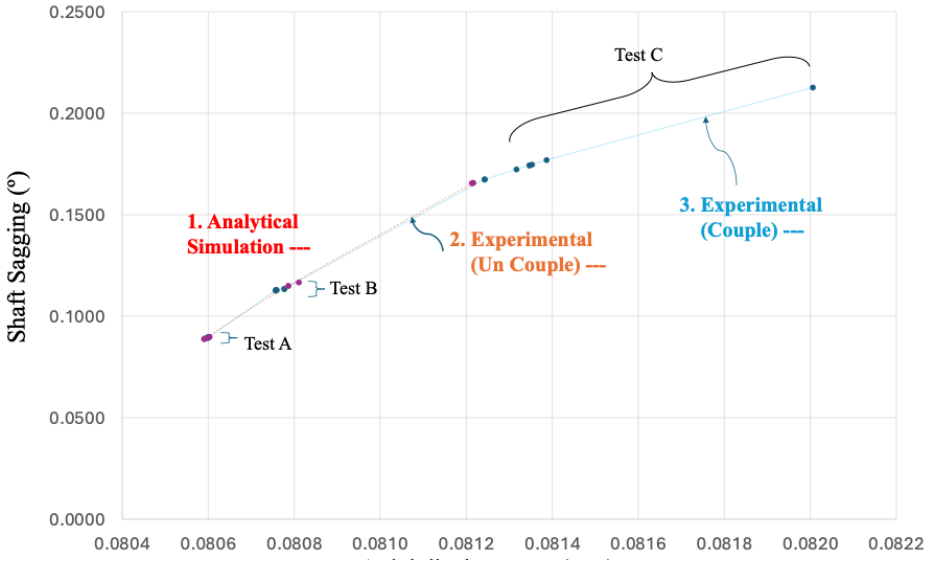

Figure 14. Shaft sagging vs air gaps – overall experimental and analytical simulation.

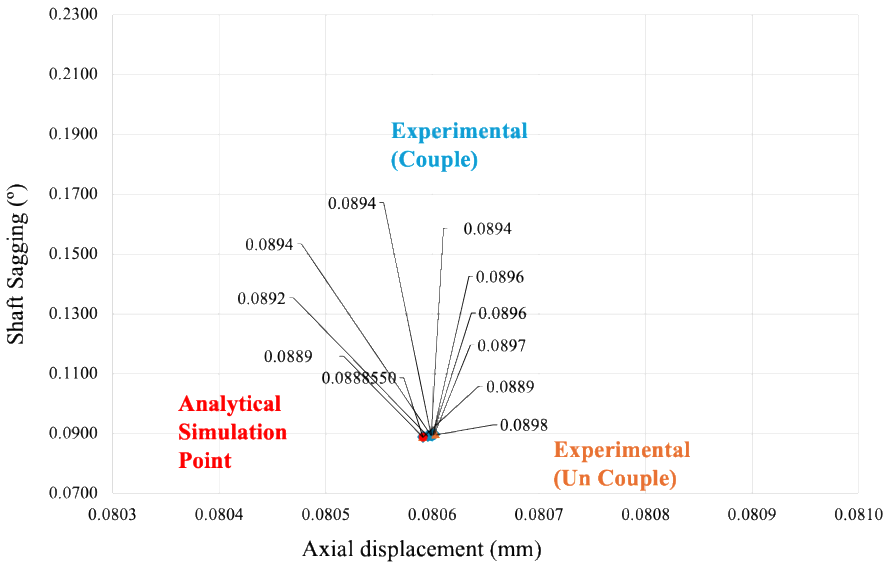

Figure 15. Shaft sagging vs air gaps – experimental and analytical simulation for test A.

4.3.2. Evaluation of test B for analytical simulation, experimental (no couple), and experimental (couple and speed)

Experimental Test B for Experimental (Couple) shows that the data characteristics are lower than those of Experimental (Un Couple), but they are concentrated around the shaft sagging between 0.1127 and 0.1149°. This suggests that there are ring misalignments occurring nearby during the rotor's response to both load and no-load conditions, as well as variations in speed, as illustrated in **Figure 16**.

From the SFF viewpoint, the system stiffness ranges from A to C. K is quantified at 65185.29 MPa, indicating the disparity in data between Experimental (Couple) and Experimental (Un Couple). The Experimental (Couple) is evaluated against the analytical simulation using an unpaired t-test. The two-tailed P value is below 0.0001, with a 95% confidence interval ranging from 0.163430 to 0.166570. The intermediate value (t) is 225.4329, accompanied by 14 degrees of freedom (df) and a standard error of difference of 0.001 mm. The hypothesis is of low value for the two-tailed P-value, suggesting that, by conventional standards, this difference is deemed highly statistically significant. The maximum vibration for the system is minimal, under 1 mm/s, indicating a smaller deflection compared to tests A and C for the rotor system. Overall evaluations indicate that the data is reliable and consistent with analytical simulations; Point B possesses adequate stiffness for PMB and is the most stable option for an overhung rotor system.

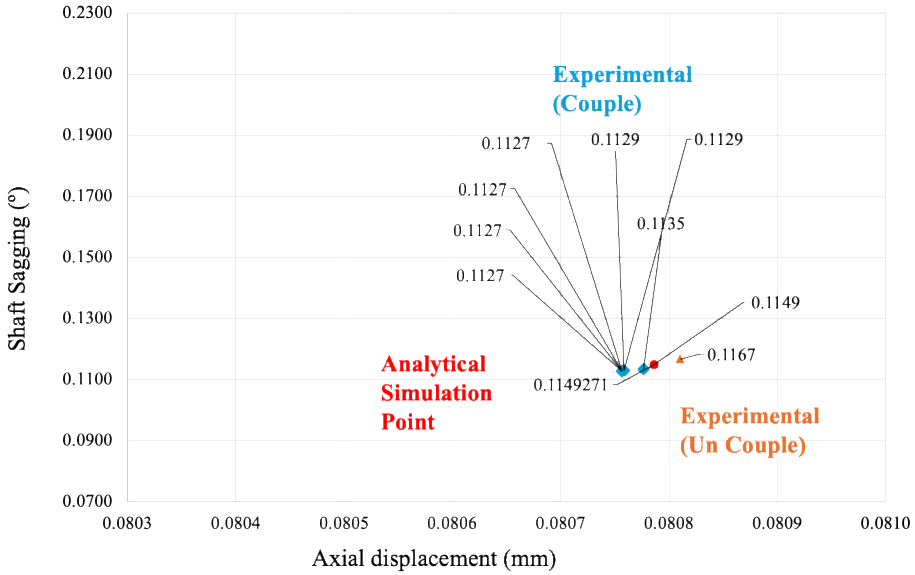

Figure 16. Shaft sagging vs air gaps – experimental and analytical simulation for test B.

4.3.3. Evaluation of test c for analytical simulation, experimental (no couple), and experimental (couple and speed)

Experimental Test C for Experimental (Couple) demonstrates that the data characteristics are positioned above the Experimental (Un Couple) for a shaft sagging of 0.1135 to 0.1152°. This indicates significant ring misalignment both under rotor load and at no-load, as well as variations in speed, as illustrated in **Figure 17**.

From the SFF point of view, the system stiffness is the lowest as compared with A and C at K is 48625.04 MPa reflects the spreading of data between Experimental (Couple) and Experimental (Un Couple). The Experimental (Couple) is compared with the analytical simulation via the implementation of an unpaired t-test. The two-tailed P value is less than

0.0001, but is rising within the 95% confidence interval range. The intermediate value (t) is 11.2749, with 14 degrees of freedom (df), and the standard error of difference is 0.026 mm. The hypothesis possesses minimal value for a two-tailed P-value, signifying that, by traditional criteria, this difference is considered highly statistically significant. The system's maximum vibration reached 2.149 mm/s during Test 18, accompanied by a significantly low air gap of 0.910 mm. Considerable deflection was observed above 5 mm at point 10 for the rotor system. Comprehensive assessments reveal that the data is dependable and aligns with analytical simulations; Point C demonstrates the lowest stiffness for PMB and signifies the most unstable configuration for the overhung rotor system.

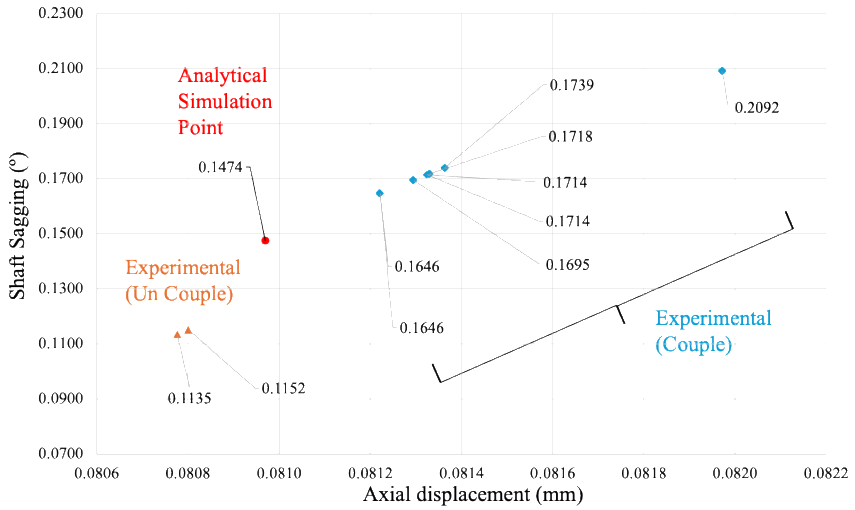

Figure 17. Shaft sagging vs air gaps – experimental and analytical simulation for test C.

4.4. Uncertainty Budget

4.4.1. Uncertainty budget for room temperature

The room temperature was measured by a Casio thermometer DQD-80J with an accuracy of ± 1°C. Twenty-eight data points were taken on three different days with an average temperature of 26.518°C. The closeness of the data points indicates that the measurement is precise, resulting in a small standard deviation of 0.09833°C. The temperature of 26.518 ± 0.09833°C is well below the operating temperature for the N35 magnet at 80°. It can be concluded that the data set shows a satisfactory laboratory measurement, accurate and precise, for influencing the uncertainty of the loss of magnetic fields (H).

4.4.2. Uncertainty budget for repeatability

The Repeatability uncertainty has been considered with a minimum of five readings for analyzing air gap, temperature, and alignment between bearings, which is above the rule of thumb for repeatability, with a minimum of 4 being sufficient.

4.4.3. Uncertainty budget for instrument

The set of instruments has been used for measuring air gaps (h1) and alignments between bearings, which depend on the accuracy of the devices. For measuring air gap (h1), shaft sagging, and PMB positions with the positioning approach, the Digital Caliper 1108-200 range of 0-200 mm has been used with an accuracy of ± 0.03 mm. The smallest increment in the vernier caliper is (1/100), equal to 0.01 mm; thus, the uncertainty for the roller is Δx = (1/2)

0.01, equal to 0.005 mm. The instrument is used to measure the air gaps (h1) and shaft sagging. It also utilized Mitutoyo 500-501-10 with an accuracy of ± 0.05 mm. The smallest increment in the vernier caliper is 1/20 mm, which is equal to 0.05 mm. Thus, the uncertainty for the roller is Δx = (1/2) 0.05, equal to 0.025 mm. The combined uncertainty for the above results is ± 0.0254951 mm, which is low and demonstrates that the measurements are accurate and precise. Shaft parallelism and bearing alignment have been used. Thus, the uncertainty Δx is equal to 0.03 mm. Another instrument used is the Mitutoyo dial gauge 513-401-10E with a resolution of 0.001 mm and an accuracy of ± 0.003 mm. The combined uncertainty is 0.063513 mm for the laboratory result, which is accurate and precise.

4.4.4. Uncertainty budget from external disturbances

The error bar in **Figure 18** relates to the accuracy of experimental data, indicating that tests 1 to 17 overlap with each other. This analysis suggests the tests are not statistically significant, as the 95% confidence intervals reflect the prediction of the analytical model and structural characteristic parameter.

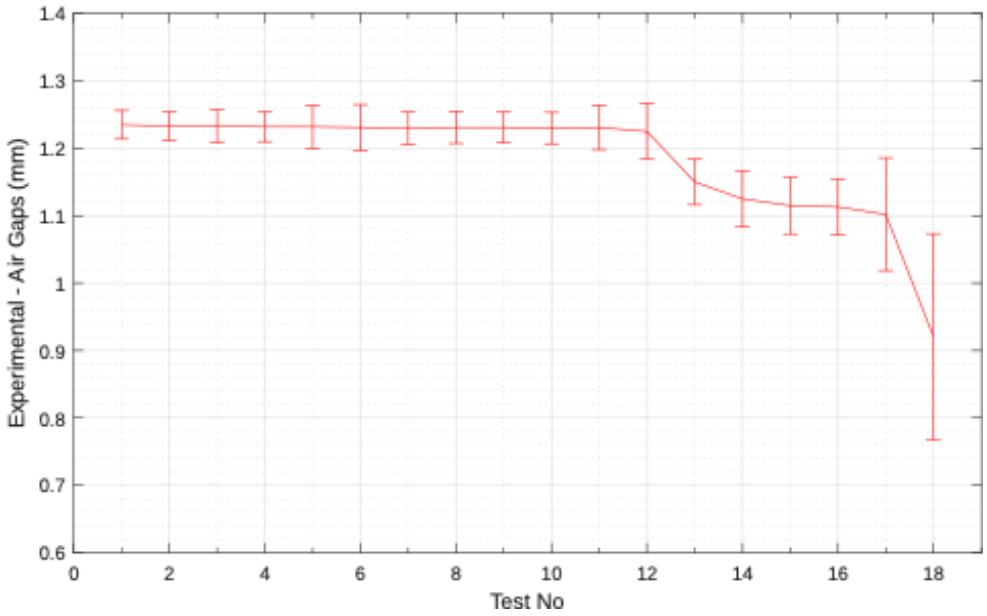

Figure 18. Error bar for tests 1 to 18.

Tests C for 13 to 18 do not overlap with test A and B, indicating the uncertainties exceed the predictions made by the analytical simulation model, that mainly influenced by external disturbances from shaft deflection and SFF.

4.4.5. Uncertainty of deflections and shaft flexibility factor (SFF) analysis for tests 13 to 18

The residual uncertainty is due to external disturbances, shaft deflection, and SFF. During no-load and load tests 13 to 18, the shaft demonstrated upward deflection, causing operation to deviate from its true center of rotation at SFF of 3930 1/m. The maximum vibrations escalated from the initiation of test 13, attaining a peak of 1.276 mm/s at 90 RPM. The increase in speed and load has heightened uncertainty due to the growing instability of the rotor, resulting in vibrations of 2.149 mm/s at 160 RPM and causing damage to the PMB rings at 250 RPM. This results in multiple issues, primarily increasing axial displacement, shaft sagging, and component stress. It is suggested that the maximum axial displacement and shaft sagging at a peak speed of 250 RPM are 0.08078 mm and 0.1135°, respectively, which can be found at test 12.

4.4.6. Uncertainty of deflections and shaft flexibility factor (SFF) analysis for tests 1 to 6

The increase in vibrations for tests 1 to 6 was due to external disturbances from shaft deflection and high stiffness from SFF. During no-load and load tests 13 to 18, the shaft demonstrated maximum deflection at the center of the rotor, causing operation to deviate from its true center of rotation at SFF of 11820 1/m. The maximum vibrations escalated from the initiation of test 1, attaining a peak of 1.110 mm/s at 90 RPM. The increase in speed and load has heightened uncertainty due to the growing instability of the rotor, resulting in vibrations of 2.240 mm/s at 250 RPM. Anyway, the result decreases during load operations due to low deflection at the middle sector of the rotor, even though the shaft sagging increases up to 0.08877° with axial displacement at 0.08060 mm. To achieve stable operations, both load and no-load have to be considered to capture the range of load reactions to PMB. It is noted that the minimum axial displacement and shaft sagging for this model at a speed of 90 RPM are 0.08075 mm and 0.08865°, respectively, which can be found at test 7.

4.5. Discussion on the Influence of Axial Displacement and Shaft Sagging on PMB Stability

The results obtained from both analytical simulations and experimental investigations demonstrate that axial displacement and shaft sagging play a critical role in determining the operational stability of PMBs in horizontal overhung systems. As shown in **Figure 13**, an increase in shaft sagging is consistently associated with a reduction in magnetic pressure due to distortion of the air gap-wavelength ratio. This behavior confirms that PMB performance is not solely governed by magnetic material properties or ring configuration, but is strongly dependent on mechanical alignment conditions, particularly under external disturbances.

The comparison between analytical simulations and experimental results, summarized in **Table 4** and illustrated in **Figure 14**, indicates that the analytical model captures the general trend of air gap reduction and shaft sagging growth with increasing axial displacement. However, a systematic offset is observed, especially at higher shaft sagging levels. This discrepancy increases almost linearly with axial displacement, suggesting that while the extended Backers-based model effectively predicts PMB behavior, residual uncertainties arise from dynamic effects that are difficult to fully represent in static analytical formulations. Similar limitations of idealized analytical PMB models have been reported in earlier studies employing magnetic scalar potential and virtual work approaches (Backers, 1960; Yonnet, 1981; Tian *et al*., 2012).

From a structural perspective, the influence of the SFF becomes increasingly dominant as axial displacement increases. The comparison among Tests A, B, and C reveals that Point B, characterized by an intermediate stiffness value, provides the most stable operational condition, as reflected by lower vibration amplitudes and more consistent air gap behavior in **Figures 15-17**. In contrast, Point A, despite having the highest stiffness, exhibits significant rotor deflection, while Point C shows pronounced instability due to insufficient stiffness. These observations align with the analytical stiffness trends presented in **Figure 10** and confirm that excessive stiffness or excessive flexibility can both degrade PMB stability.

Furthermore, the experimental vibration data indicate that increased rotational speed amplifies the combined effects of axial displacement and shaft sagging. As observed in **Table 4**, vibration amplitudes rise markedly at higher speeds, particularly for configurations with low SFF. This behavior highlights the strong coupling between mechanical dynamics and

magnetic forces in PMB systems, a factor often underestimated in earlier PMB design studies that assume quasi-static conditions (Ravaud *et al*., 2009a; Ravaud *et al*., 2009b).

Overall, the discussion confirms that incorporating axial displacement and shaft sagging into PMB design models is essential for accurately predicting real operating behavior. The agreement between analytical and experimental trends validates the proposed model, while the observed deviations emphasize the importance of considering external disturbances and shaft flexibility during early-stage PMB design. These findings provide a critical bridge between idealized PMB theory and practical engineering applications, particularly for horizontal overhung rotor systems.

4.6. Bibliometric Insights and Identified Research Gaps

Bibliometric analysis is one of the effective methods for understanding current research trends, as reported elsewhere (Nandiyanto & Al Husaeni, 2022; Nandiyanto *et al*., 2021; Solehudin *et al*., 2025). A bibliometric review of PMB-related publications reveals a strong research emphasis on stiffness enhancement, magnet configuration optimization, and numerical simulation techniques **(Figure 19)**. Analytical models based on magnetic scalar potential, virtual work, and Coulomb methods dominate the literature, while FEM-based approaches have gained increasing attention in recent years. Nevertheless, the bibliometric trends indicate a limited number of studies explicitly addressing axial displacement and shaft sagging as coupled parameters in PMB design, particularly for horizontal overhung systems. This gap underscores the need for a more comprehensive analytical framework that integrates axial displacement, shaft sagging, and shaft flexibility into PMB performance prediction. The present study directly responds to this gap by extending Backers's analytical model and validating it experimentally, thereby contributing novel insights to PMB design theory and practice.

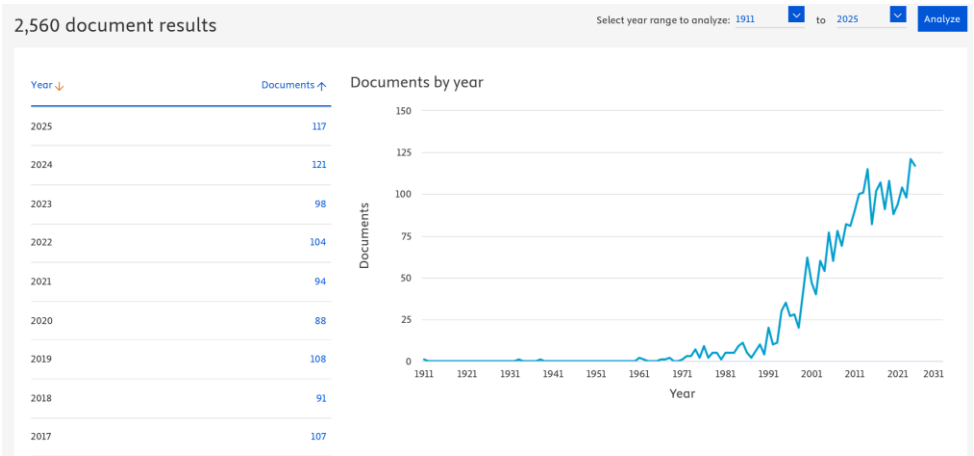

Figure 19. Bibliometric analysis regarding PMB based on the Scopus database taken in January 2026.

5. CONCLUSION

This research offers a thorough evaluation and enhancement of magnetic bearing technology. It encompasses numerous references, specifically the enhancement of existing models that integrate axial displacement and shaft sagging for optimization purposes. The research revealed that the combination of shaft sagging and axial displacement resulted in a six-fold reduction in the wavelength. This model exhibited similarity to the prior model with a 90% confidence level via equivalence testing. To achieve stability for the PMB with a shaft

diameter of Ø50.049 mm under a load ranging from 87.93 to 91.85 N, the optimal SFF is 3895 1/m, accompanied by a stiffness of 65185.29 MPa, a minimum axial displacement of 0.08075 mm, and shaft sagging of 0.08865°. The maximum axial displacement is limited to 0.08078 mm, and the shaft demonstrates a sag of 0.1135° at a peak rotational speed of 250 RPM. These parameters are crucial for mitigating uncertainty from external disturbances affecting shaft deflection, thereby ensuring the efficient operation and durability of magnetic bearings in diverse applications. Future developments may seek to improve these models to increase performance and reduce potential failures in practical applications, as outlined below.

(i) Examine the models utilized to predict the performance and efficiency of PMBs at rotational speeds of 1000, 2000, and 3000 RPM, with a SFF of 3895 per meter.
(ii) Evaluate the common external disturbances affecting temperature under various SFF, Shaft Deflection, and Shaft Sagging in dynamic conditions that contribute to the reduction of air gaps.
(iii) Establish key engineering standards to ensure the safe and reliable implementation of PMBs.
(iv) Consider potential improvements in design aimed at minimizing axial displacement and their relationship with the durability and performance of PMB.

5. ACKNOWLEDGEMENT

We wish to convey profound gratitude to Universiti Teknologi Malaysia for its support.

6. AUTHORS' NOTE

The authors declare that there is no conflict of interest regarding the publication of this article. Authors confirmed that the paper was free of plagiarism.

7. REFERENCES

Backers, F. T. (1960). A magnetic journal bearing. *Philips Tech. Rev*, *22*(7), 232-238.

Lijesh, K.P., Muzakkir, S.M., and Hirani, H. (2016). Failure mode and effect analysis of passive magnetic bearing. *Engineering Failure Analysis*, *62*(1), 1–20.

Moser, R., Sandtner, J., and Bleuler, H. (2006). Optimization of repulsive passive magnetic bearings. *IEEE Transactions on Magnetic*s, *42*(8), 2038–2042.

Nandiyanto, A. B. D., Al Husaeni, D. N., and Al Husaeni, D. F. (2021). A bibliometric analysis of chemical engineering research using vosviewer and its correlation with covid-19 pandemic condition. *Journal of Engineering Science and Technology*, *16*(6), 4414-4422.

Nandiyanto, A. B. D., and Al Husaeni, D. F. (2022). Bibliometric analysis of engineering research using vosviewer indexed by Google Scholar. *Journal of Engineering Science and Technology*, *17*(2), 883-894.

Paden, B., Groom, N., and Antaki, J. (2003). Design formulas for permanent-magnet bearings, *Journal of Mechanical Design*, *125*(4), 734-738.

Ravaud, R., Lemarquand, G., and Lemarquand, V. (2009a). Force and stiffness of passive magnetic bearings using permanent magnets. Part 1: axial magnetization. *IEEE Transactions on Magnetics*, *45*(7), 2996–3002.

Ravaud, R., Lemarquand, G., and Lemarquand, V. (2009b). Force and stiffness of passive magnetic bearings using permanent magnets. Part 2: radial magnetization. *IEEE Transactions on Magnetics*, *45*(9), 3334–3342.

Solehuddin, M., Nandiyanto, A. B. D., Muktiarni, M., Rahayu, N. I., Al Husaeni, D. N., Ragadhita, R., and Fiandini, M. (2025). Engineering research and scientific contributions at Universitas Pendidikan Indonesia: Trends, challenges, and future directions. *Journal of Engineering Science and Technology*, *20*(3), 816-836.

Tian, L.L., Ai, X.P., and Tian, Y.Q. (2012). Analytical model of magnetic force for axial stack permanent-magnet bearings. *IEEE Transactions on Magnetics*, *48*(10), 2592–2599.

Wang, J., Wang, D., Tong, S., Sun, T., Li, L., Kong, W., Zhong, D., and Sun, H. (2023). A review of recent developments in permanent Magnet Eddy Current Couplers technology. *Actuators*, *12*(7), 277.

Yonnet, J. P. (1981) Permanent magnet bearing and coupling. *Magnetics, IEEE Transactions*, *17*, 1169 - 1173.

Zhang, L.I., Huachun, P., Wu, Y., Li, H., and Song, C. (2019). Design, analysis, and experiment of multiring permanent magnet bearings by means of equally distributed sequences based monte carlo method. *Mathematical Problems in Engineering*, *2019*(1),1-17.

Zhang, W., Pan, W., and Yang, Z. (2011). Finite element method analysis and digital control for radial AC hybrid magnetic bearings. *Journal of Computational &Theoretical Nanoscience*, *4*(8), 2869–2874.